HHS Public Access

Author manuscript

Bioconjug Chem. Author manuscript; available in PMC 2019 October 25.

Published in final edited form as:

Bioconjug Chem. 2018 November 21; 29(11): 3746–3756. doi:10.1021/acs.bioconjchem.8b00636.

Tuning Pharmacokinetics to Improve Tumor Accumulation of a Prostate-Specific Membrane Antigen-Targeted Phototheranostic Agent

Kara M. Harmatys[†,‖,#], **Marta Overchuk**[†,‡,#], **Juan Chen**[†], **Lili Ding**[†], **Ying Chen**[§], **Martin G. Pomper**[§], **Gang Zheng**[*,†,‡,‖]

[†]Princess Margaret Cancer Centre, University Health Network, 101 College Street, Toronto, Ontario M5G 1L7, Canada

[‡]Institute of Biomaterials and Biomedical Engineering, University of Toronto, 164 College Street, Toronto, Ontario M5S 3G9, Canada

[§]Johns Hopkins Medical School, 1550 Orleans Street, 492 CRB II, Baltimore, Maryland 21287, United States

[‖]Department of Medical Biophysics, University of Toronto, 101 College Street, Toronto, Ontario M5G 1L7, Canada

Abstract

We describe a simple and effective bioconjugation strategy to extend the plasma circulation of a low molecular weight targeted phototheranostic agent, which achieves high tumor accumulation (9.74 ± 2.26%ID/g) and high tumor-to-background ratio (10:1). Long-circulating pyropheophorbide (LC-Pyro) was synthesized with three functional building blocks: (1) a porphyrin photosensitizer for positron-emission tomography (PET)/fluorescence imaging and photodynamic therapy (PDT), (2) a urea-based prostate-specific membrane antigen (PSMA) targeting ligand, and (3) a peptide linker to prolong the plasma circulation time. With porphyrin's copper-64 chelating and optical properties, LC-Pyro demonstrated its dual-modality (fluorescence/PET) imaging potential for selective and quantitative tumor detection in subcutaneous, orthotopic, and metastatic murine models. The peptide linker in LC-Pyro prolonged its plasma circulation time about 8.5 times compared to its truncated analog. High tumor accumulation of LC-Pyro enabled potent PDT, which resulted in significantly delayed tumor growth in a subcutaneous xenograft model. This approach can be applied to improve the pharmacokinetics of existing and future targeted PDT agents for enhanced tumor accumulation and treatment efficacy.

Graphical Abstract

[*]Corresponding Author gang.zheng@uhnres.utoronto.ca.
[#]Kara M. Harmatys and Marta Overchuk have contributed equally to the manuscript.

Supporting Information

The Supporting Information is available free of charge on the ACS Publications website at DOI: 10.1021/acs.bioconjchem.8b00636. Flow cytometry, fluorescence mouse imaging and biodistribution, ^{64}Cu-LC-Pyro PET/CT imaging and organ gamma counting, PDT histological organ toxicity, blood clearance of YC-9 (PDF)

The authors declare no competing financial interest.

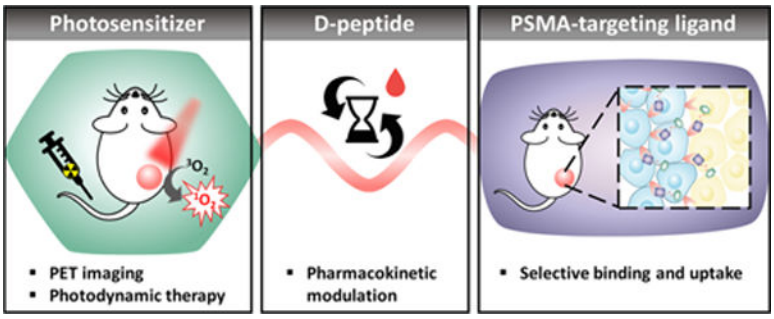

BACKGROUND

Photodynamic therapy (PDT) has emerged as a highly effective tool for cancer ablation without the use of ionizing radiation and with minimal off-target toxicity.[1] The mechanism of PDT relies on the generation of reactive oxygen species (ROS) with a combination of a photosensitizer, light, and oxygen.[2] Current photosensitizers can be separated as hydrophilic agents that clear rapidly and act intravascularly or hydrophobic agents that accumulate in the tissues.[3] Nonspecific uptake of hydrophobic photosensitizers results in off-target light toxicity, which limits the utility of this approach. One way to reduce off-target toxicity and improve photosensitizer tumor accumulation is to design a cancer cell-targeted agent that would confine ROS generation selectively to cancer cells.

Prostate specific membrane antigen (PSMA) has recently attracted significant attention in the oncology community due to the success of PSMA-targeted nuclear imaging and therapeutic radionuclide delivery, which is beginning to affect management of patients with prostate cancer.[4–7] PSMA is a type II transmembrane glycoprotein that is highly overexpressed in prostate cancer. Its expression positively correlates with cancer aggressiveness.[8–10] A variety of PSMA-targeted photosensitizers have appeared recently.[7,11–16] For example, Chen et al. developed a small-molecule PSMA-targeted photosensitizer,[11] while Nagaya et al. conjugated a near-infrared photosensitizer to a monoclonal antibody.[17] While the low-molecular-weight photosensitizer enables deep tumor tissue penetration and fast targeting kinetics, its rapid clearance resulted in a suboptimal efficacy, explaining the need for multiple reinjections followed by PDT. On the contrary, the antibody-based photosensitizer exhibited a long plasma circulation time and favorable biodistribution,[18] but poor tissue penetration due to high molecular weight may limit its therapeutic potential.[19] To address limitations of existing PSMA-targeted photosensitizers we designed an agent that combines the virtues of low molecular weight (<2 kDa) and synthetic accessibility demonstrated by small molecules, while maintaining the long circulation time characteristic of antibody-photosensitizer conjugates.

The designed agent consists of a pyropheophorbide *a* photosensitizer, a highly selective PSMA-binding ligand and a peptide-based pharmacokinetic modulator[20] (Figure 1). We demonstrate that the insertion of a peptide linker significantly prolongs its plasma circulation time and ultimately enhances its tumor accumulation. This enables efficient single-dose photodynamic treatment, while inherent fluorescence and ^{64}Cu-chelating porphyrin properties allows multimodal imaging (PET/fluorescence) of prostate cancer.

RESULTS AND DISCUSSION

LC-Pyro Synthesis and Characterization.

We developed a PSMA-targeted phototheranostic agent that consists of three functional building blocks: (1) a porphyrin capable of multimodal fluorescence/PET imaging and photodynamic activity, (2) a 9-amino-acid D-peptide linker to impart water-solubility and improve the plasma circulation time, and (3) a urea-based high-affinity PSMA as a targeting ligand (Figure 1). LC-Pyro (Long-circulating pyropheophorbide *a*) and SC-Pyro (Short-circulating pyropheophorbide *a*) were synthesized and confirmed by UPLC-MS analysis with identified ESI+ mass spectrometry and corresponding UV–vis absorption (Figure 2A and Figure S1). LC-Pyro (*m*/*z* calculated $[M]^+$ 1835.99, found $[M]^+$ 1836.3, $[M]^{2+}$ 918.0); SC-Pyro (*m*/*z* calculated $[M]^+$ 1119.33, found $[M]^+$ 1119.4, $[M]^{2+}$ 559.6). DCIBzL was previously synthesized and was used as an inhibitor ligand *in vitro* and *in vivo* to confirm PSMA specificity.[21] LC-Pyro absorbance (Figure 2B) and fluorescence (Figure 2C) were collected and its measured photodynamic activity revealed an increase in generation of ROS with an increase in laser light dose up to 5 J/cm^2 (Figure 2D). Next, for PET imaging and quantitative biodistribution studies, we chelated ^{64}Cu to LC-Pyro and evaluated its radiochemical purity by radio-HPLC. The corresponding HPLC traces demonstrated peak alignment of porphyrin absorbance and ^{64}Cu radioactivity, indicating effective ^{64}Cu labeling of LC-Pyro with no remaining free ^{64}Cu (Figure 2E).

PSMA Affinity Ligand Demonstrates High Targeting Specificity.

Targeted uptake of a photosensitizer by biomarker-overexpressing cancer cells can introduce an additional level of selectivity for PDT. Western blots in Figure 3A validated PSMA expression in the primary or metastatic lines (ML) modified to express high (PSMA+ PC3 PIP; PC3- ML-1124) or low (PSMA- PC3 flu; PC3-ML-1117) levels of PSMA. As cell-penetrating properties of porphyrins[22] might contribute to LC-Pyro intracellular uptake *in vitro* beyond the PSMA-mediated pathway (Figure S2), we synthesized a FITC-labeled analog (LC-FITC) to investigate the targeting selectivity of the peptide-PSMA moiety. Fluorescence microscopy of LC-FITC in Figure 3B revealed selective membrane staining in PC3 prostate cells overexpressing PSMA (PSMA+ PC3 PIP), whereas negligible fluorescence was observed in cells with low PSMA expression (PSMA- PC3 flu) under equivalent incubation settings (3 μM, 3 h) and exposure time. LC-FITC also localized to one focus within the perinuclear region, which has been observed previously and described to represent the mitotic spindle poles or an endosomal compartment.[23] Addition of 100× excess DCIBzL to LC-FITC achieved successful PSMA binding inhibition, indicating target specificity of the conjugated small-molecule ligand. LC-FITC selectivity was confirmed by flow cytometry over 22 h. Fluorescence intensity from LC-FITC uptake increased in a time-dependent manner in PSMA+ PC3 PIP cells with a 15-fold higher uptake than PSMA- PC3 flu cells (Figure 3C).

Peptide Linker Prolongs Plasma Circulation Time Enhancing Tumor Accumulation of LC-Pyro.

To validate the pharmacokinetic role of the peptide linker in LC-Pyro and its ability to accumulate in PSMA+ tumors, we synthesized a truncated derivative, SC-Pyro, where the 9-

amino-acid peptide sequence was replaced by a single lysine residue. Results in Figure 4A demonstrated that LC-Pyro exhibited an 8.5-fold longer plasma circulation time ($t_{1/2,\ slow}$ = 10.00 h; $t_{1/2,\ fast}$ = 0.50 h) than SC-Pyro ($t_{1/2,\ slow}$ = 1.17 h; $t_{1/2,\ slow}$ = 0.20 h). To ensure that the *in vivo* targeting results were not affected by any difference in binding affinity, the inhibitory activities of LC-Pyro, SC-Pyro, and DCIBzL against PSMA were determined using a fluorescence-based assay. All three compounds demonstrated subnanomolar inhibitory capacity, despite conjugation of the porphyrin peptide linker to the PSMA inhibitor resulting in an order of magnitude lower PSMA inhibitory properties than DCIBzL (Figure 4B). The specificity of LC-Pyro to PSMA was confirmed in a subcutaneous PSMA+ PC3 PIP xenograft model by inhibition with excess DCIBzL. Excised PSMA+ PC3 PIP tumors revealed less accumulation of LC-Pyro when DCIBzL (PSMA blocker) was injected 30 min beforehand (Figure 4C). Additionally, the PSMA target specificity *in vivo* was validated with LC-Pyro absent the PSMA affinity ligand. Mice bearing dual subcutaneous PSMA- PC3 flu and PSMA+ PC3 PIP tumors were injected with LC-Pyro (-PSMA affinity ligand) followed by whole-animal *in vivo* fluorescence imaging (Figure S3). Negligible accumulation of probe within both the PSMA- and PSMA+ tumors was observed after 24 h. Next, to assess the influence of the plasma circulation time between LC-Pyro and SC-Pyro on tumor accumulation and biodistribution, equivalent doses of each agent were intravenously administered to mice bearing dual subcutaneous PSMA- PC3 flu and PSMA+ PC3 PIP tumors followed by whole-animal *in vivo* fluorescence imaging over 24 h. Figure 4D shows a strong diffuse fluorescence signal from LC-Pyro after 1 h with selective accumulation to the PSMA+ tumor after 24 h. There is negligible accumulation within both the PSMA- and PSMA+ tumors 24 h post-administration of SC-Pyro (Figure 4E and Figure S4), indicating the importance of long plasma circulation time for successful tumor accumulation. *Ex vivo* organ distribution in Figure 4F reveals liver and kidney clearance of LC-Pyro, whereas a majority of SC-Pyro was metabolized and collected in the gallbladder (Figure 4G). That suggests that SC-Pyro cleared rapidly from the body, and therefore, a much higher dose or multiple doses would be required to achieve comparable tumor accumulation to LC-Pyro after 24 h. *Ex vivo* organ distribution of LC-FITC after 24 h shows similar organ distribution to LC-Pyro, confirming the role of peptide linker in the clearance pathway of the conjugates (Figure S5).

Multimodal Imaging of PSMA+ Prostate Cancer.

After validating targeting of LC-Pyro in a subcutaneous PSMA+ PC3 PIP tumor model, we explored its theranostic application in two different mouse models bearing either a primary prostate tumor or metastatic prostate cancer. Due to the intrinsic metal-chelation properties of porphyrin ring structures, LC-Pyro was chelated to ^{64}Cu, which allowed for *in vivo* PET imaging and biodistribution.[24] As demonstrated in Figure 5A and Figure S6 with PET/CT imaging, ^{64}Cu-LC-Pyro delineated the orthotopic PSMA+ PC3 PIP tumor 17 h post-injection, whereas the PSMA- PC3 flu tumor did not have significant uptake. Biodistribution revealed over 4-fold selective accumulation in PSMA+ PC3 PIP tumor [9.74 ± 2.26 percentage injected dose per gram of tissue (%ID/g)] vs 2.30 ± 0.09%ID/g in the PSMA- PC3 flu tumor, which showed no distinguishable signal from the surrounding healthy prostate tissue or pelvic organs (Figure 5B and Table S1). ^{64}Cu-LC-Pyro accumulated greatest in the liver, kidney, and feces, indicative of hepatobiliary and renal clearance.

To investigate further the potential of LC-Pyro to accumulate selectively in PSMA-expressing malignant tissues, we performed fluorescence imaging of micrometastasis. *In situ* fluorescence images of fluc+/PSMA+ (PC3-ML-1124) and fluc+/PSMA- (PC3-ML-1117) tumors demonstrated selective uptake of LC-Pyro in the PSMA+ tumor nodule (Figure 5C). Those observations aligned with the previous data obtained in subcutaneous xenografts. Following *in situ* fluorescence imaging, further verification of LC-Pyro accumulation in metastatic nodules and the surrounding tissues was examined by fluorescence microscopy of DAPI-stained tissue sections. Robust porphyrin fluorescence signal in the PSMA+ metastatic nodule microstructure was observed. Notably, the surrounding muscle tissue demonstrated fluorescence near to that of background, further supporting PSMA+ cell selectivity of LC-Pyro.

PDT with LC-Pyro Results in Significantly Delayed Tumor Growth.

We evaluated the therapeutic potential of LC-Pyro by performing *in vivo* LC-Pyro-enabled PDT in the PSMA+ PC3 PIP subcutaneous tumor model. Optimization (data not shown) indicated a dose of 100 J/cm^2 fluence to be appropriate, which is within the clinically relevant dose range. In mice injected with LC-Pyro and treated by light, significant swelling was observed in the tumor region 24 h after PDT. Approximately 4 days after treatment, mice in the LC-Pyro + Laser group developed scarring in the tumor region, which was completely healed by day 22 (Figure 6C). No therapeutic effect was observed in the animals treated with saline, LC-Pyro without laser exposure, or laser alone. Importantly, animals injected with LC-Pyro with no laser treatment revealed no sign of skin phototoxicity upon daylight exposure. Overall, significant tumor growth inhibition was observed in the LC-Pyro + Laser group compared to the control cohorts (Figure 6A), with no decrease in body weight (Figure 6B). After day 22, tumor regrowth was observed in two animals, most likely from an insufficient laser irradiation area, limited by the maximum beam spot diameter in the custom-built optical setup. The two remaining animals demonstrated no signs of residual or recurrent disease 44 days post-PDT.

Acute cytotoxic effects of PSMA-targeted PDT were confirmed in a separate animal cohort, where PSMA+ PC3 PIP subcutaneous tumors and organs were harvested 24 h post-PDT treatment. H&E staining revealed significant damage of tissue architecture in the LC-Pyro + Laser group, while tumors harvested from the other control groups revealed high tumor cell density and intact cellular structure (Figure 6D). TUNEL staining confirmed the presence of significant cell death in the LC-Pyro + Laser group. No acute damage to major organs was observed as confirmed by histology (Figure S7).

Our results indicate that the insertion of a 9-amino-acid D- peptide linker between a porphyrin photosensitizer and a PSMA-targeting small-molecule ligand extends its plasma circulation time 8.5-fold compared to its truncated analog. This allows for repeated passages of the agent through the tumor vasculature, increasing the probability of extravasation and active PSMA binding and cell internalization. Improved plasma circulation time of the agent resulted in efficient single-dose PDT compared to the repeated treatments necessary with a previously reported PSMA photosensitizer, YC-9, with a faster blood clearance (Figure S9). The use of a pharmacokinetic modulator to extend the plasma circulation time holds the

potential to enhance the efficacy of other targeted cancer therapies, such as radioimmunotherapy and activatable agents within the tumor microenvironment. Additionally, this strategy could be universally applied to the design of theranostic agents targeting alternative cancer-specific biomarkers beyond PSMA.

CONCLUSIONS

In summary, LC-Pyro is a versatile, long-circulating, PSMA-targeted phototheranostic agent. The embedded peptide linker extended its plasma circulation time up to 10.00 h compared to its truncated derivative (1.17 h), resulting in a remarkably high tumor accumulation (9.74 ± 2.26%ID/g). Favorable pharmacokinetics and of LC-Pyro in combination with its targeted PSMA binding led to the effective single-dose tumor ablation by PDT in a PSMA+ PC3 PIP subcutaneous mouse model. Radiolabeling of LC-Pyro with ^{64}Cu enabled PET imaging, which can be used for precision treatment planning. LC-Pyro also proved effective for fluorescence-based detection of PSMA + metastatic nodules, which is important for image-guided surgical resection or palliative PDT.

MATERIALS AND METHODS

The activating agent (benzotriazol-1-yl)-*N,N,N′,N′*-tetramethyluronium hexafluorophosphate (HBTU) was purchased from Novabiochem (Etobicoke, ON, Canada), and used without further purification. The Rink amide resins and all 9*H*-fluoren-9-ylmethoxycarbonyl (N-Fmoc)-protected amino acids were purchased from Novabiochem. Pyropheophorbide *a* and urea-based PSMA inhibitor containing an *N*-hydroxysuccinamide (NHS) moiety were synthesized by the previous described protocols.[25,26] Cell culture medium was obtained from ATCC (American Type Culture Collection, Manassas, VA). FBS and trypsin-ethylenediaminetetraacetic acid (EDTA) solution were purchased from Gibco (Invitrogen Co, Waltham, MA). $^{64}CuCl_2$ was obtained from Washington University (St. Louis, MO).

Synthesis and Characterization of Pyro-peptide-PSMA (LC-Pyro) and Pyro-k-PSMA (SC-Pyro).

A peptide sequence with D-amino acid backbone, Fmoc-gd(OtBu)e(OtBu)vd(OtBu)gs(tBu)gk(Mtt), was synthesized on Rink resin using Fmoc chemistry protocol. After removing the last Fmoc group, Pyro acid was coupled to the N-terminal of the peptide on resin at room temperature ([Pyro acid/HBTU/ peptide 3:3:1]). The Pyro-peptide-resin was then treated with a cleavage cocktail (TFA: triisopropylsilane: water = 95:2.5:2.5) for 1 h at room temperature to remove the resin and cleave the protected groups. The acquired Pyro-peptide (Pyro-gdevdgsgk(NH_2)) was conjugated with PSMA-NHS (Pyro-peptide/PSMA-NHS/DIPEA, 1:1.2:2) in anhydrous DMSO. The acquired Pyro-peptide-PSMA (LC-Pyro) was purified by HPLC. Pyro-k-PSMA (SC-Pyro) was synthesized in a similar way with the peptide linker replaced by a single lysine linker. The synthesis of LC-Pyro and SC-Pyro were confirmed with UPLC-MS analysis with identified ESI mass spectrometry and corresponding UV–vis absorption (Figure S1). LC-Pyro (*m*/*z* calculated for $C_{86}H_{118}N_{18}O_{27}$ $[M]^+$ 1835.99, found $[M]^+$ 1836.3, $[M]^{2+}$ 918.0); SC-Pyro (*m*/*z* calculated for $C_{59}H_{78}N_{10}O_{12}$) $[M]^+$1119.33, found $[M]^+$ 1119.4, $[M]^{2+}$ 559.6). Reverse-

phase analytical UPLC–MS were performed on a ACQUITY UPLC BEH C18 column (1.7 μm, 2.1 mm × 50 mm) using a Waters 2695 controller with a 2996 photodiode array detector and a Waters TQ mass detector. The conditions were as follows: solvent (A) 0.1% trifluoroacetic acid (TFA); (B) acetonitrile; column temperature: 60 °C; flow rate: 0.6 mL/min gradient: from 60% A + 40% B to 0% A + 100% B in 3 min, kept at 100% B for 1 min, followed by a sharp change back to 60% A + 40% B and a hold for another 1 min. A fluorescence spectrum of LC-Pyro was acquired on a Fluoromax-4 fluorometer (Horiba Jobin Yvon, NJ).

Reactive Oxygen Species Generation of LC-Pyro.

Reactive oxygen species generation of LC-Pyro was measured using a commercially available Amplex UltraRed Reagent (AUR) assay (Thermo Fisher Scientific). The $OD_{665\ nm}$ of LC-Pyro in 70:30 MeOH:PBS was set to 0.15 and was added in a black clear-bottom 96-well plate. AUR was dissolved in DMSO (10 mM) and diluted 100-fold in each well. The wells were then irradiated by a 671 nm laser (DPSS LaserGlow Technologies) at increasing light doses (0.5, 1.0, 2.0, 3.0, and 5.0 J/cm^2). Fluorescence emission of the fluorogenic product of AUR was measured (excitation: 550 nm; emission: 581 nm) using a ClarioStar microplate reader (BMG LABTECH).

Ligand Binding Affinity of LC-Pyro, SC-Pyro, and DCIBzL.

The inhibitory activities of LC-Pyro, SC-Pyro, and DCIBzL against PSMA were determined using a fluorescence-based assay according to a previously reported procedure.[27] Briefly, lysates of LNCaP cells (25 μL in 0.1 M Tris-HCl, pH 8.0) were incubated with the serial dilutions of the test compounds (in 12.5 μL of 0.1 M Tris-HCl, pH 8.0) in the presence of 4 μM *N*-acetylaspartylglutamate (NAAG) (in 12.5 μL of 0.1 M Tris-HCl, pH 8.0) for 120 min. The reaction mixtures were incubated with the working solution (50 μL) of the Amplex Red Glutamic Acid Kit (Molecular Probes Inc., Eugene, OR) for 60 min. The amount of glutamate released from NAAG hydrolysis by the LNCaP lysates was determined by measuring the fluorescence generated from the reactions using the Cytation 5 plate reader (BioTek, Winooski, VT) with excitation at 545 nm and emission at 590 nm. Inhibition curves were determined using semilog plots, and IC_{50} values were determined at the concentration at which enzyme activity was inhibited by 50%. Enzyme inhibitory constants (K_i values) were generated using the Cheng-Prusoff conversion.[28] Data analysis was performed using GraphPad Prism software ($n = 3$).

^{64}Cu Radiolabeling.

LC-Pyro (225 nmol) was dissolved in 18 μL of DMSO and saline was added then vortexed, producing a dark green solution (450 μM). $^{64}Cu(Cl)_2$ solution (pH = 5.5; ~5.0 mCi; 0.5 mL) was then added and the reaction mixture was heated in a water bath at 60 °C for 30 min. After radiolabeling was completed, sample was diluted with 1 mL of saline and the radiochemical purity was analyzed by instant thin layer chromatography (iTLC). Briefly, a 1 cm × 8 cm strip of heat-activated glass microfiber chromatography paper (Aligent Technologies, USA) was spotted with 2 μL of sample 1.5 cm from the bottom of the strip. The strip was then placed into a capped test tube containing mobile phase prepared with 2 vol % EDTA (Sigma-Aldrich Co. LLC) and 10 vol % 0.1 M NH_4OAc in ddH_2O. The

retention value of nonchelated ^{64}Cu was reproducibly greater than 0.9. The developed iTLC strip was cut in thirds and the ^{64}Cu radioactivity assayed for the two top (free ^{64}Cu) and separately for a bottom piece (^{64}Cu-LC-Pyro) using a Wizard 1480 well-type automatic gamma counter (PerkinElmer Inc.; Shelton, CT, USA) and radiochemical purity was further evaluated by radio HPLC performed on a XBridge-C18 column (2.5 μm, 4.6 mm × 50 mm) with UV detector and radioactivity detector Figure S. Further purification of ^{64}Cu-LC-Pyro was deemed unnecessary, due to the high molar ratio of LC-Pyro:$^{64}CuCl_2$ (~1000:1) and its high radiochemical purity. In addition, previous reports indicate that copper chelation into a porphyrin ring did not significantly change the *in vivo* uptake and clearance profiles.[29]

In Vitro Targeting and Cellular Uptake.

All cell lines (PSMA+ PC3 PIP, PSMA- PC3 flu, PC3-ML-1124, and PC3- ML-1117) were cultured in RPMI-1640 medium (Invitrogen, Carlsbad, CA) containing 10% FBS (Invitrogen) and 1% penicillin-streptomycin (Biofluids, Camarillo, CA).[9,30] Cell cultures were maintained in a 37 °C humidified incubator under 5% CO_2. PSMA expression for all tested cell lines was validated with western blot analysis. For fluorescence microscopy experiments, PSMA+ PC3 PIP and PSMA- PC3 flu cells were seeded into 8-well coverglass-bottom chambers (Nunc Lab-Tek, Sigma–Aldrich, Rochester, NY) at a cell-seeding density of 2 × 104 cells per well. After 24 h of incubation, medium was replaced with 3 μM LC-FITC (1 vol % DMSO in medium) and incubated for 3 h. For inhibition studies, the known PSMA inhibitor, DCIBzL, was added in molar excess (100×) in combination with 3 μM LC-FITC for 3 h. Fluorescence imaging was performed on an Olympus IX73 inverted microscope using a 60× magnification objective. LC-FITC signal was detected using a FITC filter (excitation: 485/ 20 nm bandpass; emission: 522/24 nm) and Hoechst nuclear stain was detected using a DAPI filter (excitation: 387/11 nm bandpass; emission 447/60 nm). Images were processed using ImageJ software. For flow cytometry studies, PSMA+ PC3 PIP and PSMA- PC3 flu cells were seeded in 6-well plates at a cell density of 5×10^5 cells per well. After 24 h, cells were replaced with fresh medium and treated with 2 μM LC-FITC for 0.5, 1, 3, 5, and 22 h. After incubation, cells were trypsinized, centrifuged and washed two times, resuspended in 0.5 mL FACS buffer (0.5 mM EDTA and 5 mg/L DNase in PBS) and filtered. Quantification of the fluorescence signal was performed using a Beckman Coulter FC500 five-color analyzer and FITC fluorescence was detected (FITC channel, excitation: 505 nm LP; emission: 530/30 nm) for 10,000 counts. The exact protocol was applied to LC-Pyro incubation conditions (7AAD channel, excitation: 635 nm LP; emission: 660/20 nm). Median fluorescence was subtracted from cells with no LC-FITC treatment and histogram plots were generated using FlowJo software.

Xenograft Mouse Models.

Animal studies were conducted under institutional approval (University Health Network, Toronto, Canada). For generation of subcutaneous tumor xenografts, athymic male nude mice under general anesthesia (2 vol % isoflurane in oxygen) were inoculated with 2.5×10^6 PSMA+ PC3 PIP or PSMA- PC3 flu cells in 60 μL of saline into the right or left flank. An orthotopic prostate tumor model was generated as described elsewhere.[31] Briefly, 2.5×10^6 PSMA+ PC3 PIP or PSMA- PC3 flu cells in 20 μL of saline were injected to the dorsal

prostate lobe using a 28- gauge needle, animals were sutured back and administered with 0.1 mg/kg of bupenorphine for analgesia. Orthotopic prostate tumor growth was monitored by magnetic resonance imaging (MRI, Biospec 70/30 USR, Bruker, Billerica, MA). For the metastatic prostate cancer model, 2×10^6 PC3-ML- 1124 (PSMA+; fluc+) or PC3-ML-1117 (PSMA-; fluc+) cells in 200 μL of saline were administered via lateral tail vein.[32] Development of metastatic nodules was monitored by bioluminescence imaging (Xenogen, Caliper Life Sciences, Hopkinton, MA) every 3 days.

For the targeting studies *in vivo*, animals bearing PSMA- PC3 flu (left flank) and PSMA+ PC3 PIP (right flank) subcutaneous tumors ($n = 3$) were injected intravenously with 20 nmol of LC-Pyro in 0.2 mL of saline (1 vol % DMSO) and imaged with a CRi Maestro imaging system (Caliper Life Sciences, Waltham, MA) with 680 nm excitation and 700 nm detection (integration time = 500 ms) at 0.5, 1, 3, 6, and 24 h post-injection. After 24 h, animals were sacrificed and tumors were excised for *ex vivo* imaging. For inhibition studies *in vivo*, animals bearing a single PSMA+ PC3 PIP tumor were injected with 15 nmol of LC-Pyro with a second cohort receiving an intravenous injection of PSMA inhibitor (DCIBzL, 155× molar excess) 30 min prior to LC-Pyro injection ($n = 3$). A lower dose of LC-Pyro (15 nmol) was chosen to minimize the total dose of DCIBzL due to its decreased water solubility at high concentrations. Animals were sacrificed 24 h post-injection and tumors were excised and imaged *ex vivo*. Relative difference in fluorescence accumulation was calculated using ImageJ software.

Pharmacokinetics and Qualitative Fluorescence Biodistribution Studies.

For the pharmacokinetic studies, LC-PSMA, SC-PSMA, and YC-9[11] ($n = 5$ each cohort), were intravenously injected into healthy BALB/c mice at the dose of 20 nmol per animal. Blood was collected from the saphenous vein prior to injection of probe and at 5 min, 0.5, 1, 2, 4, 8, 24, and 48 h post-injection. Blood samples were then centrifuged for 10 min at 10,000 rpm and the collected plasma fraction was diluted 50× in DMSO. Fluorescence intensity for Pyro (excitation: 630 nm; emission: 650–750 nm) and YC-9 (excitation: 620 nm; emission: 650–850 nm) was measured by Fluoromax-4 spectrofluorometer (Horiba Scientific, NJ) and normalized integrated peak values were analyzed by Graphpad Prism to calculate the half-life of each compound. For qualitative biodistribution studies animals bearing dual PSMA+ PC3 PIP and PSMA- PC3 flu subcutaneous tumors were injected with SC-Pyro, LC-Pyro, or LC-Pyro absent the PSMA affinity ligand (20 nmol) and images were analyzed using software from the CRi Maestro imaging system.

PET/CT Imaging and Biodistribution of Mouse Xenografts.

Mice bearing PSMA PC3 PIP ($n = 4$) or PSMA- PC3 flu ($n = 3$) orthotopic prostate tumors were administered with ^{64}Cu -LC-Pyro solution (0.2 mL, 1 vol % DMSO, ~0.5 mCi, 25 nmol of LC-Pyro). PET/CT imaging was performed on one animal from each group at 3 and 17 h post-injection on a small-animal MicroPET system (Focus 220: Siemens, Munich, Germany) with CT coregistration on a microCT system (Locus Ultra: GE Healthcare, U.K.). Twenty-four hour post-injection of ^{64}Cu-LC-Pyro, animals were euthanized via cardiac puncture under 2% isoflurane anesthesia. Organs of interest, including the tumor, prostate, seminal vesicles, testes, heart, spleen, lungs, liver, kidneys, adrenal, stomach, small intestine,

large intestine, skin, fat, muscle, bone, and brain were excised, washed in saline, dried with absorbent tissue, weighed, and radioactivity was measured on a Wizard 1480 well-type automatic gamma counter (PerkinElmer Inc.; Shelton, CT). Radioactivity measured in each organ was decay-corrected and expressed as the percentage of the injected dose per gram of tissue (% ID/g).

Fluorescence Detection of Prostate Metastasis.

Animals with PSMA+ (PC3-ML-1124) or PSMA- (PC3-ML-1117) firefly luciferase-expressing metastatic lesions were administered with 20 nmol of LC-Pyro (0.2 mL saline, 1 vol % DMSO) via tail vein injection. Twenty-four hours post-injection animals received 60 mg/kg of luciferin intraperitoneally and were sacrificed 10 min later via cervical dislocation. Internal organs were removed to expose the metastatic nodules present in retroperitoneal cavity alongside bioluminescent imaging to detect the exact location of the metastases. Fluorescent imaging was conducted *in situ* and *ex vivo* using a CRi Maestro imaging system (616 to 661 nm bandpass excitation and 675 nm long-pass emission optical interference filters; integration time = 500 ms). The nodules were excised with the surrounding muscle tissue, placed in optical cutting temperature (OCT) compound and snap-frozen in liquid nitrogen vapor. Sections at 10 μm thickness were cut, deparaffinized, and stained with DAPI-containing mounting medium. Fluorescence imaging of tissue slices was performed on an Olympus IX73 inverted microscope using a 20× magnification objective. LC-Pyro signal was detected using a Cy5 filter (excitation: 628/40 nm bandpass; emission: 692/40 nm) and DAPI signal was detected using a DAPI filter (excitation: 387/11 nm bandpass; emission: 447/60 nm). Images were pseudocolored and the intensity was scaled using CellSens software (Olympus Canada Inc.).

Photodynamic Therapy.

Mice bearing one subcutaneous PSMA+ PC3 PIP flank tumor were randomly divided into four groups: (1) saline only, (2) LC-Pyro only, (3) laser only, and (4) LC-Pyro + laser (n = 4). Animals in group 2 and group 4 were intravenously injected with 50 nmol and 30 nmol of LC-Pyro, respectively. LC-Pyro uptake was monitored by *in vivo* fluorescence imaging for 6 h, followed by tumor laser treatment for mice in groups 3 and 4. Using a 671 nm free-space laser (DPSS LaserGlow Technologies), tumors were treated with a single PDT light dose of 100 J/cm^2 (0.63 cm^2 laser spot area; fluence rate 55 mW/cm^2). Body weight was recorded and tumor volumes were measured with calipers using the equation V_{tumor} = 1/2 (length × width × width). Topical antibiotic Flamazine was applied to the tumors in group 4 after day 2, due to typical scarring that results from PDT treatment. Animals were removed from the experiment and sacrificed when the tumor reached >1000 mm^3 or started ulcerating, as stated under the animal care institutional guidelines.

Statistical Analysis.

A two-tailed Student's t test was used to determine statistical significance. P-values less than 0.05 were considered significant.

Supplementary Material

Refer to Web version on PubMed Central for supplementary material.

ACKNOWLEDGMENTS

The authors would like to acknowledge Lili Ding for performing western blots and assisting with flow cytometry measurements; Dr. Il Minn for PSMA binding affinity Ki value measurements; Deborah Scollard, Teesha Komal, and Dr. Nicholas Bernards for help with PET/CT image acquisition and reconstruction and Dr. Warren Folz for MR images (STTARR Innovation Centre); Dr. Raymond Reilly, Dr. Zhongli Cai, and Dr. Conrad Chan for the assistance with radio-HPLC. This study was funded by the Terry Fox Research Institute (PPG#1075), the Canadian Institute of Health Research (Foundation Grant #154326), the Canadian Cancer Society Research Institute (704718), the Vanier Canada Graduate Scholarship, the Canada Foundation for Innovation, the Joey and Toby Tanenbaum/Brazilian Ball Chair in Prostate Cancer Research, Prostate Cancer Canada, Natural Sciences, and Engineering Research Council of Canada, the Princess Margaret Cancer Foundation, and NIH grants CA134675, CA184228, CA202199, and EB024495.

ABBREVIATIONS

LC-Pyro	Long-circulating pyropheophorbide
a	prostate-specific membrane antigen
PET	positron emission tomography
PDT	photodynamic therapy
kDa	kilodaltons
ROS	reactive oxygen species
SC-Pyro	short-circulating pyropheophorbide *a*
UPLC-MS	ultraperformance liquid chromatography mass spectrometry
ESI	electrospray ionization
HPLC	high-performance liquid chromatography
J/cm^2	Joules per square centimeter
ML	metastatic line
PC3	prostate cancer cell line
LC-FITC	long-circulating fluorescein isothiocyanate
SD	standard deviation
$t_{1/2}$	half-life
K_i	inhibitor constant
PET/CT	positron emission tomography/computed tomography
%ID/g	percent injected dose per gram

fluc	firefly luciferase
DAPI	4′,6-diamidino-2-phenylindole
H&E	Hematoxylin & Eosin
TUNEL	Terminal deoxynucleotidyl transferase dUTP nick end labeling
HBTU	(benzotriazol-1-yl)-*N,N,N′,N′*-tetramethyluronium hexafluorophosphate
Fmoc	Fluorenylmethyloxycarbonyl protecting group
NHS	*N*-hydroxysuccinamide
FBS	fetal bovine serum
EDTA	ethylenediaminetetraacetic acid
DMSO	dimethyl sulfoxide
FACS	Fluorescence-activated cell sorting
PBS	phosphate buffered saline
MRI	magnetic resonance imaging
OCT	optical cutting temperature
mg/kg	milligrams per kilogram
LP	long-pass
rpm	revolutions per minute
mCi	millicuries
Cy5	cyanine 5

REFERENCES

(1). Cengel KA, Simone CB II, and Glatstein E. (2016) PDT: What's Past Is Prologue. Cancer Res 76 (9), 2497–2500. [PubMed: 27197260]

(2). Wilson BC, and Patterson MS. (2008) The physics, biophysics and technology of photodynamic therapy. Phys. Med. Biol 53 (9), R61–R109. [PubMed: 18401068]

(3). Ethirajan M, Chen Y, Joshi P, and Pandey RK. (2011) The role of porphyrin chemistry in tumor imaging and photodynamic therapy. Chem. Soc. Rev 40 (1), 340–362. [PubMed: 20694259]

(4). Haberkorn U, Eder M, Kopka K, Babich JW, and Eisenhut M. (2016) New Strategies in Prostate Cancer: Prostate-Specific Membrane Antigen (PSMA) Ligands for Diagnosis and Therapy. Clin. Cancer Res 22 (1), 9–15. [PubMed: 26728408]

(5). Kratochwil C, Bruchertseifer F, Giesel FL, Weis M, Verburg FA, Mottaghy F, Kopka K, Apostolidis C, Haberkorn U, and Morgenstern A. (2016) 225Ac-PSMA-617 for PSMA-Targeted a-Radiation Therapy of Metastatic Castration-Resistant Prostate Cancer. J. Nucl. Med 57, 1941–1945. [PubMed: 27390158]

(6). Kratochwil C, Giesel FL, Stefanova M, Beneě M, Bronzel M, Afshar-oromieh A, Mier W, Eder M, Kopka K, and Haberkorn U. (2016) PSMA-Targeted Radionuclide Therapy of Metastatic

Castration-Resistant Prostate Cancer with 177Lu-Labeled PSMA-617. J. Nucl. Med 57 (8), 1170–1177. [PubMed: 26985056]

(7). Wang X, Tsui B, Ramamurthy G, Zhang P, Meyers J, Kenney ME, Kiechle J, Ponsky L, and Basilion JP. (2016) Theranostic Agents for Photodynamic Therapy of Prostate Cancer by Targeting Prostate-Specific Membrane Antigen. Mol. Cancer Ther 15 (8), 1834–1844. [PubMed: 27297866]

(8). Bostwick DG, Pacelli A, Blute M, Roche P, and Murphy GP. (1998) Prostate Specific Membrane Antigen Expression in Prostatic Intraepithelial Neoplasia and Adenocarcinoma. Cancer 82, 2256–2261. [PubMed: 9610707]

(9). Kiess AP, Minn I, Vaidyanathan G, Hobbs RF, Josefsson A, Shen C, Brummet M, Chen Y, Choi J, Koumarianou E, Baidoo K, Brechbiel MW, Mease RC, Sgouros G, Zalutsky MR, and Pomper MG. (2016) (2S)-2-(3-(1-Carboxy-5-(4–211At-Astatobenzamido)Pentyl)Ureido)-Pentanedioic Acid for PSMA-Targeted -Particle Radiopharmaceutical Therapy. J. Nucl. Med 57 (10), 1569–1575. [PubMed: 27230930]

(10). Israeli RS, Powell CT, Corr JG, Fair WR, and Heston WDW. (1994) Expression of the Prostate-specific Membrane Antigen. Cancer Res 54, 1807–1811. [PubMed: 7511053]

(11). Chen Y, Chatterjee S, Lisok A, Minn I, Pullambhatla M, Wharram B, Wang Y, Jin J, Bhujwalla ZM, Nimmagadda S, Mease RC, and Pomper MG. (2017) A PSMA-targeted theranostic agent for photodynamic therapy. J. Photochem. Photobiol., B 167, 111–116. [PubMed: 28063300]

(12). Fakhrejahani F, Madan RA, and Dahut WL. (2017) Management Options for Biochemically Recurrent Prostate Cancer. Curr. Treat. Option. On 18 (5), 26.

(13). Liu T, Wu LY, and Berkman CE. (2010) Prostate-specific membrane antigen-targeted photodynamic therapy induces rapid cytoskeletal disruption. Cancer Lett 296 (1), 106–112. [PubMed: 20452720]

(14). Liu T, Wu LY, Choi JK, and Berkman CE. (2009) In vitro targeted photodynamic therapy with a pyropheophorbide-a conjugated inhibitor of prostate-specific membrane antigen. Prostate 69, 585–594. [PubMed: 19142895]

(15). Nagaya T, Nakamura Y, Okuyama S, Ogata F, Maruoka Y, Choyke PL, and Kobayashi H. (2017) Near-Infrared Photoimmunotherapy Targeting Prostate Cancer with Prostate-Specific Membrane Antigen (PSMA) Antibody. Mol. Cancer Res. 15 (9), 1153–1162. [PubMed: 28588059]

(16). Serrell EC, Pitts D, Hayn M, Beaule L, Hansen MH, and Sammon JD. (2018) Review of the comparative effectiveness of radical prostatectomy, radiation therapy, or expectant management of localized prostate cancer in registry data. Urol. Oncol-Semin. Ori 36, 1–10.

(17). Nakajima T, Mitsunaga M, Bander N, Heston WD, Choyke PL, and Kobayashi H. (2011) Targeted, Activatable, In Vivo Fluorescence Imaging of Prostate-specific Membrane Antigen (PSMA)-positive Tumors Using the Quenched Humanized J591 Antibody-ICG Conjugate. Bioconjugate Chem 22 (8), 1700–1705.

(18). Watanabe R, Hanaoka H, Sato K, Nagaya T, Harada T, and Mitsunaga M. (2015) Photoimmunotherapy Targeting Prostate-Specific Membrane Antigen: Are Antibody Fragments as Effective as Antibodies? J. Nucl. Med 56 (1), 140–145. [PubMed: 25500827]

(19). Minchinton AI, and Tannock IF. (2006) Drug penetration in solid tumours. Nat. Rev. Cancer 6 (8), 583–592. [PubMed: 16862189]

(20). Stefflova K, Li H, Chen J, and Zheng G. (2007) Peptide-based pharmacomodulation of a cancer-targeted optical imaging and photodynamic therapy agent. Bioconjugate Chem 18 (2), 379–388.

(21). Chandran SS, Banerjee SR, Mease RC, Pomper MG, and Denmeade SR. (2008) Characterization of a targeted nanoparticle functionalized with a urea-based inhibitor of prostate-specific membrane antigen (PSMA). Cancer Biol. Ther 7 (6), 974–982. [PubMed: 18698158]

(22). Chen Y, Gryshuk A, Achilefu S, Ohulchansky T, Potter W, Zhong T, Morgan J, Chance B, Prasad PN, Henderson BW, Oseroff A, and Pandey RK. (2005) A Novel Approach to a Bifunctional Photosensitizer for Tumor Imaging and Phototherapy. Bioconjugate Chem 16, 1264–1274.

(23). Kiess AP, Minn I, Chen Y, Hobbs R, Sgouros G, Ronnie C, Pullambhatla M, Shen CJ, Foss CA, and Martin G. (2015) Auger Radiopharmaceutical Therapy Targeting Prostate-Specific Membrane Antigen. J. Nucl. Med 56 (9), 1401–1407. [PubMed: 26182968]

(24). Shi J, Liu TW, Chen J, Green D, Jaffray D, Wilson BC, Wang F, and Zheng G. (2011) Transforming a Targeted Porphyrin Theranostic Agent into a PET Imaging Probe for Cancer. Theranostics 1, 363–370. [PubMed: 21938264]

(25). Zheng G, Li H, Zhang M, Lund-Katz S, Chance B, and Glickson JD. (2002) Low-density lipoprotein reconstituted by pyropheophorbide cholesteryl oleate as target-specific photosensitizer. Bioconjugate Chem 13 (3), 392–396.

(26). Chandran SS, Banerjee SR, Mease RC, Pomper MG, and Denmeade SR. (2008) Characterization of a targeted nanoparticle functionalized with a urea-based inhibitor of prostate-specific membrane antigen (PSMA). Cancer Biol. Ther 7 (6), 974–982. [PubMed: 18698158]

(27). Chen Y, Dhara S, Banerjee SR, Byun Y, Pullambhatla M, Mease RC, and Pomper MG. (2009) A low molecular weight PSMA-based fluorescent imaging agent for cancer. Biochem. Biophys. Res. Commun 390 (3), 624–629. [PubMed: 19818734]

(28). Cheng Y, and Prusoff WH. (1973) Relationship between the inhibition constant (K1) and the concentration of inhibitor which causes 50% inhibition (I50) of an enzymatic reaction. Biochem. Pharmacol 22 (23), 3099–3108. [PubMed: 4202581]

(29). Wilson BC, Firnau G, Jeeves WP, Brown KL, and Burns-McCormick DM. (1988) Chromatographic analysis and tissue distribution of radiocopper-labelled haematoporphyrin derivatives. Lasers in Medical Science 3 (1), 71–80.

(30). Chang SS, Reuter VE, Heston WDW, Bander NH, Grauer LS, and Gaudin PB. (1999) Five Different Anti-Prostate-specific Membrane Antigen (PSMA) Antibodies Confirm PSMA Expression in Tumor-associated Neovasculature 1. Cancer Res No. 212, 3192–3198.

(31). Jin CS, Overchuk M, Cui L, Wilson BC, Bristow RG, Chen J, and Zheng G. (2016) Nanoparticle-Enabled Selective Destruction of Prostate Tumor Using MRI-Guided Focal Photothermal Therapy. Prostate 76 (13), 1169–1181. [PubMed: 27198587]

(32). Castanares MA, Copeland BT, Chowdhury WH, Liu MM, Rodriguez R, Pomper MG, Lupold SE, and Foss CA. (2016) Characterization of a novel metastatic prostate cancer cell line of LNCaP origin. Prostate 76 (2), 215–225. [PubMed: 26499105]

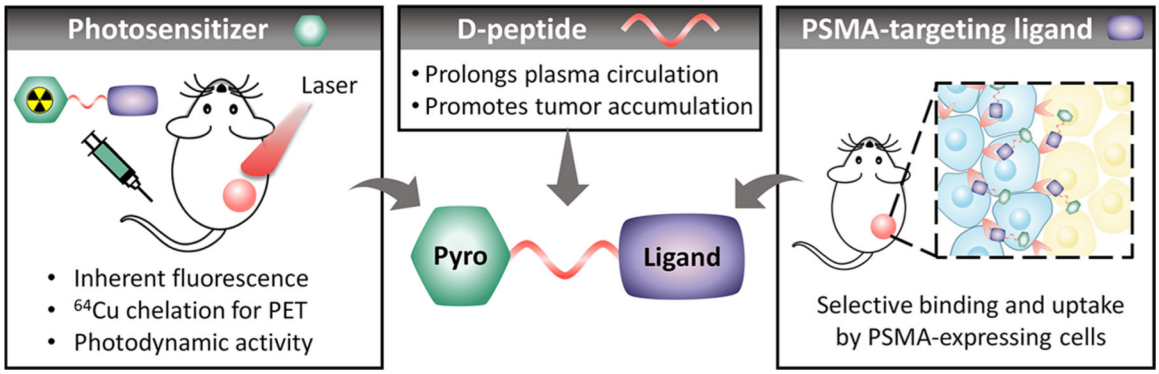

Figure 1.

Schematic structure of the theranostic probe LC-Pyro (long-circulating pyropheophorbide *a*), which is comprised of three building blocks: (1) a porphyrin photosensitizer capable of deep-red fluorescence imaging and ^{64}Cu chelation for PET imaging; (2) a 9-amino acid D-peptide sequence that imparts water-solubility and prolongs plasma circulation to promote tumor accumulation; and (3) a high-affinity urea-based small-molecule PSMA targeting ligand.

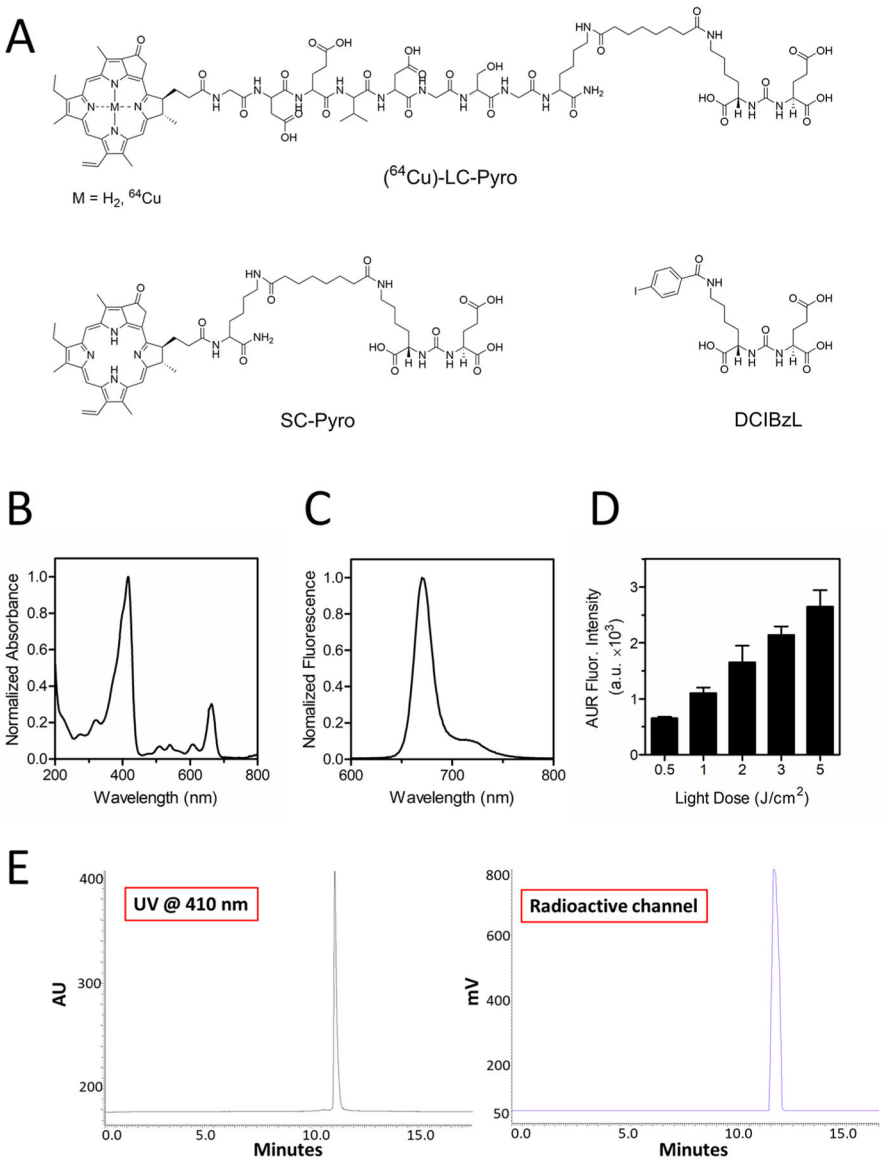

Figure 2.

Structures of PSMA conjugates, the photonic properties of LC-Pyro, and the radio-HPLC trace of ^{64}Cu-LC-Pyro. (A) Structures of LC-Pyro (Long-circulating pyropheophorbide *a*), SC-Pyro (Short-circulating pyropheophorbide *a*) and DCIBzL. (B) LC-Pyro absorbance spectrum and (C) fluorescence emission spectrum. (D) Reactive oxygen species generation from LC-Pyro in solution with respect to 671 nm laser light dose (n = 3 from three independent measurements). (E) Evaluation of radiochemical purity of ^{64}Cu-labeled LC-Pyro by radio-HPLC monitored by absorption at 410 nm (left, LC-Pyro signal) and by radioactive detector (^{64}Cu signal). The only peak at a retention time of 11 min showed both 410 nm and radioactive signal indicated high purity of ^{64}Cu-labeled LC-Pyro.

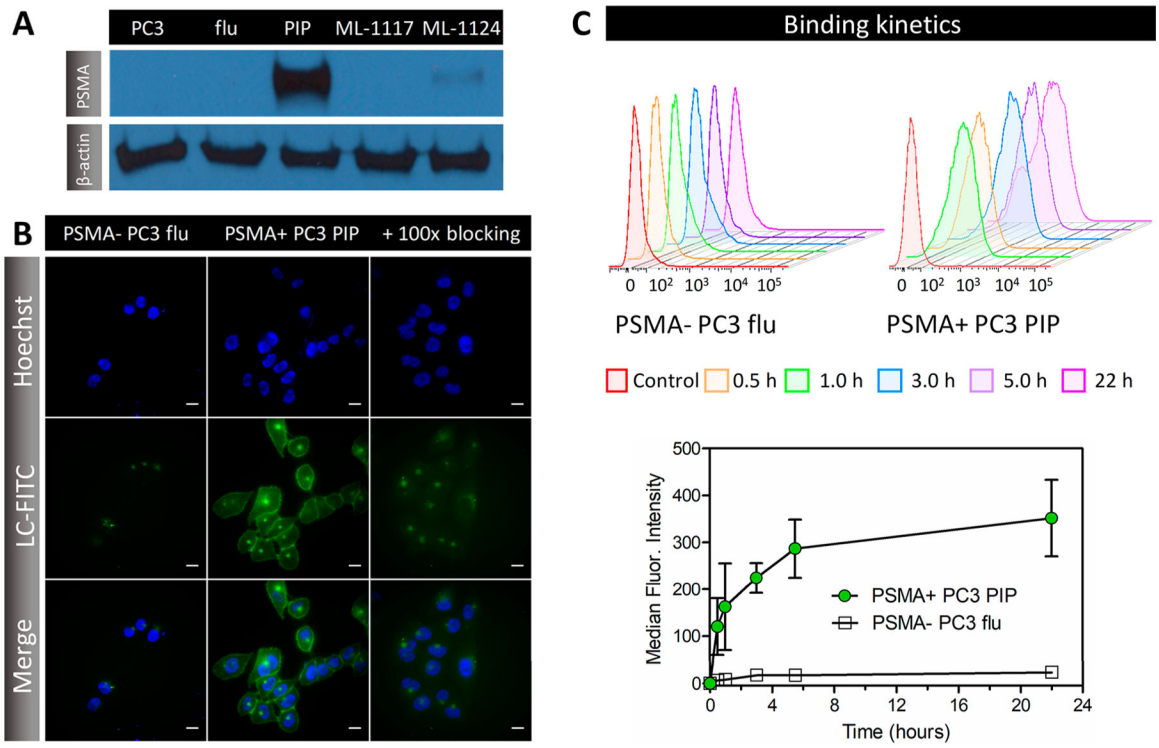

Figure 3.

PSMA targeting selectivity and specificity *in vitro*. (A) Western blots of PC3, PSMA- PC3 flu, PSMA+ PC3 PIP, PC3- ML-1117, and PC3- ML-1124 cell lysates using anti-PSMA and β-actin antibodies. (B) Representative fluorescence micrographs of LC-FITC (3 μM, 3 h incubation) uptake in PSMA- PC3 flu and PSMA+ PC3 PIP cells in the presence of 100× excess DCIBzL for target blockade. Scale = 25 μm. (C) Representative flow cytometry histogram plots with time-dependent quantification of LC-FITC uptake in PSMA- PC3 flu (open black square) and PSMA+ PC3 PIP (solid green circle) cells. Each point represents the median ± SD of three independent measurements.

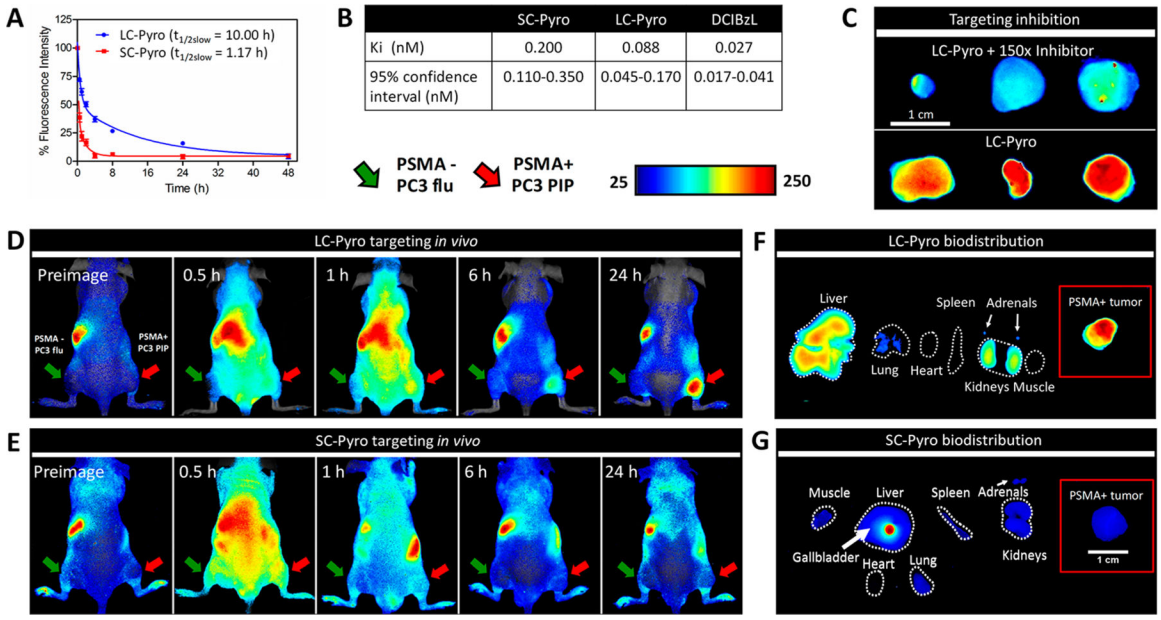

Figure 4.

Pharmacokinetic role of the peptide linker in LC-Pyro for its ability to accumulate in PSMA-expressing tumors. (A) Blood clearance curves of LC-Pyro and SC-Pyro (n = 5 each group) in BALB/c mice with blood samples collected over 48 h. The profiles fit into a two-compartment model with a half-life of 10.00 h for LC-Pyro and 1.17 h for SC-Pyro. (B) Table including the K_i inhibitory activities of SC-Pyro, LC-Pyro, and DCIBzL against PSMA determined using a fluorescence-based assay. (C) PSMA inhibition *in vivo* with 150× molar excess of DCIBzL intravenously injected 30 min prior to LC-Pyro intravenous injection. Mice were sacrificed 24 h post-injection and tumors were excised for *ex vivo* fluorescence comparison. (D) Representative fluorescence images of mice bearing dual PSMA+ PC3 PIP (red arrow) and PSMA- PC3 flu (green arrow) tumors that were intravenously injected either with LC-Pyro or (E) SC-Pyro at 0.5, 1, 6, and 24 h post-injection. (F) Fluorescence *ex vivo* organ distribution of mice injected with LC-Pyro or (G) SC-Pyro including PSMA+ PC3 PIP tumor (insets). All images displayed are comparable with the same integration time.

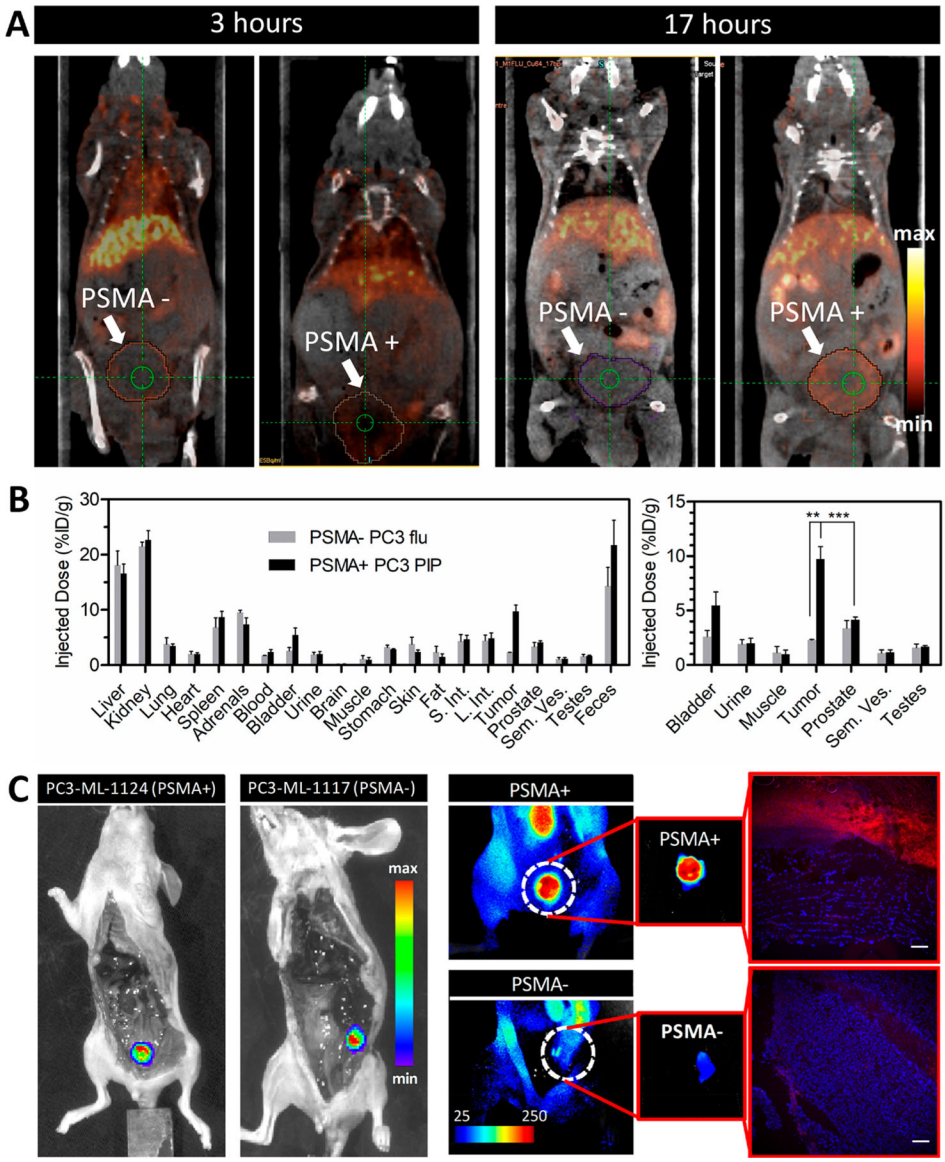

Figure 5.

^{64}Cu-LC-Pyro-enabled PET imaging in an orthotopic prostate cancer model and fluorescence detection of PSMA+ micrometastases with LC-Pyro. (A) Sagittal PET/CT images from one mouse bearing either a PSMA+ PC3 PIP or PSMA- PC3 flu orthotopic prostate tumor at 3 and 17 h after intravenous administration of ^{64}Cu -LC-Pyro. (B) ^{64}Cu-labeled LC-Pyro biodistribution in the tumors and the surrounding organs quantified via gamma counting ($n = 4$ for PSMA+ PC3 PIP; $n = 3$ for PSMA- PC3 flu, $^{**}P < 0.01$; $^{***}P < 0.001$). (C) *In situ* bioluminescence images of mice bearing PSMA+ (PC3-ML-1124) and PSMA- (PC3-ML-1117) metastatic nodules (internal organs removed, to expose retroperitoneal cavity). Corresponding fluorescence images demonstrating specific uptake of LC-Pyro in the PSMA+ nodule and the fluorescence microscopic analysis of 10 μm frozen sections (LC-Pyro, red; DAPI, blue; scale = 20 μm).

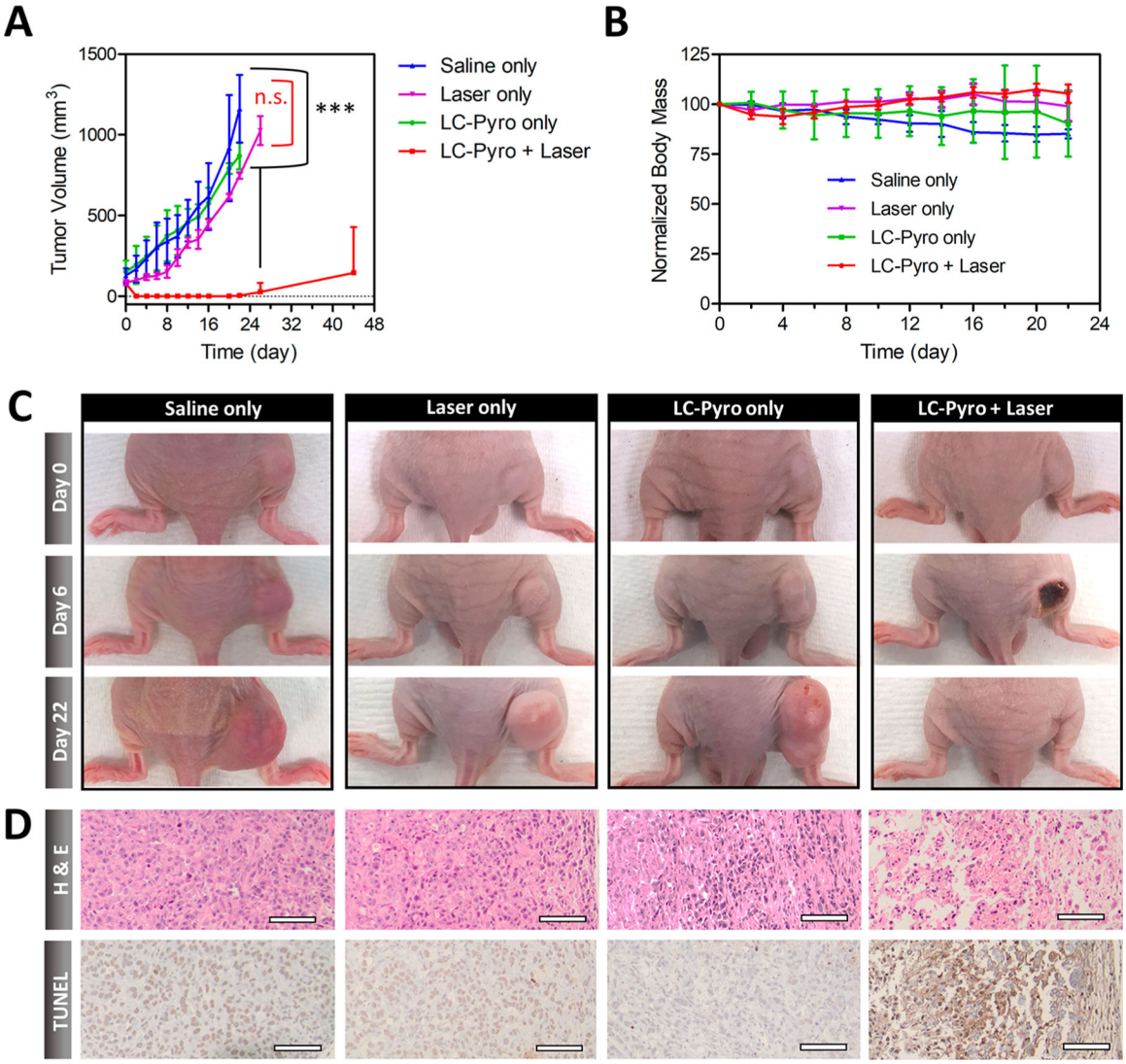

Figure 6.

PDT efficacy of LC-Pyro in PSMA+ PC3 PIP subcutaneous tumor-bearing mice. (A) Tumor growth curves represented as average tumor volume ± standard deviation ($n = 4$ for each group, ***$P \leq 0.001$, n.s. = not significant). (B) Body mass curves (mean ± SD). (C) Representative images of tumor-burdened mice in four treatment groups: (1) saline only, (2) laser only, (3) LC-Pyro only, and (4) LC-Pyro + Laser at 0, 6, and 22 days post-PDT treatment. (D) H&E and TUNEL staining of tumor sections from saline only, laser only, LC-Pyro only, and LC-Pyro + Laser groups at 24 h post-treatment; scale = 50 μm.